J Nanostruct 16(3): 3497-3505, Summer 2026

RESEARCH PAPER

Sol–Gel Auto-Combustion Synthesis of ZnS Nanoparticles and Their Influence on the Thermal Conductivity and Mechanical Performance of Epoxy Nanocomposites

Hind W. Abdullah *, F. Y Mohammed, Zahraa J. Hamakhan, Sarah A. Jasim, N.A. Hassan, Khalil Taha Jadaan

Department of Physics, College of Science, University of Diyala, Diyala, Iraq

ARTICLE INFO

Article History:
Received 22 March 2026
Accepted 20 May 2026
Published 01 July 2026

Keywords:
Epoxy nanocomposites
Mechanical properties
Sol–gel auto-combustion synthesis
Thermal conductivity
ZnS nanoparticles

ABSTRACT

A series of ZnS semiconductor nanoparticles were synthesized successfully by sol–gel method with zinc nitrate and thiourea as precursors of Zn and S, respectively. X-ray diffraction (XRD) analysis confirmed the formation of a cubic crystalline phase. Diffraction peaks A-C had the lattice parameter values (a) were 5.349, 5.374 and 5.383 Å respectively which shows good agreement with usual cubic ZnS structure. The crystallite size was found to be 28.549 nm, confirming the nanocrystalline nature of the prepared sample. The strain (ε) values were found to be 0.0013, 0.00095, and 0.0018 for the main diffraction peaks, indicating slight lattice distortion in the synthesized nanoparticles. FESEM was used to determine the particle size and surface morphology of the synthesized ZnS nanoparticles, revealing nearly spherical particles with noticeable agglomeration and an average particle size of around 66.87 nm. Epoxy/ZnS nanocomposites were hand-lay-up at room temperature, ZnS nanoparticles was added at (0, 1.5, 3, 4.5, and 6) wt%. Adding ZnS nanoparticles to epoxy significantly increases thermal conductivity (from 0.42 to ~0.89 W·m−1·K−1) as filler loading rises (0–6 wt%). Finally, epoxy/ZnS nanocomposites were a sustainability application, thermally conductive, durable encapsulates for photovoltaic (solar) modules to improve heat dissipation, extend module lifetime, and increase energy yield.

How to cite this article
Abdullah H., Mohammed F., Hamakhan Z., Jasim S., Hassan N., Jadaan K. Sol–Gel Auto-Combustion Synthesis of ZnS Nanoparticles and Their Influence on the Thermal Conductivity and Mechanical Performance of Epoxy Nanocomposites. J Nanostruct, 2026; 16(3):3497-3505. DOI: 10.22052/JNS.2026.03.041

INTRODUCTION

In recent years, nanostructured semiconductor materials have received growing attention owing to the emergence of quantum confinement effects, which impart remarkable optical and electrical characteristics [1–3]. Among the large family of II–VI semiconductors, zinc sulfide (ZnS) represents a particularly interesting material for numerous applications like light-emitting devices [4], phosphor technology [5] and nonlinear optical systems [6], as well as in the fields of pharmacy [7], electroluminescent devices [8] and fluorescence sensing platforms [9,10]. The synthesis conditions, especially the temperature, are crucial for controlling the particle size and morphology of ZnS nanostructures [12]. The particle size relies on a balance between kinetic and thermodynamic factors. Temperature plays a

* *Corresponding Author Email: hindwaleed@uodiyala.edu.iq*

very important role in changing the mechanisms of particle growth; Particle growth, such as Ostwald ripening, depends on several parameters (diffusion processes, interfacial energy, kinetic conditions that leads to sampling and solubility equilibrium) [13]. In addition, the preparation method is critical to determining the structural and physical properties of ZnS materials. Numerous synthesis methods have been investigated like chemical spray pyrolysis [14], solvothermal routes [15], successive ionic layer adsorption and reaction (SILAR) method [16] and pulsed laser deposition [17], metal-organic chemical vapor deposition (MOCVD) method [18,19] and thermal evaporation [20–22]. However, due to the unremitting creation and miniaturization of electronic devices, highly developed materials with improved thermal management features should be in high demand [23]. High efficiency for heat dissipation is critical to keep operational stability, reliability, and safety in many energy storage systems including electric vehicles and high-performance battery modules. Due to their exceptional mechanical strength, processing capabilities, thermal resistance and endurance to corrosive environment [24], epoxy resins. However, the relatively low thermal conductivity of this type of material (around 0.19 W/mK) lowers their performance in heat transfer applications [25]. As a result, the introduction of nanoscale fillers to enhance thermal conductivity has gradually become one successful way for polymer-based composites. Recently, nanoparticles have been used as reinforcing agents to improve mechanical integrity and chemical stability of epoxy systems [26]. These fillers can successfully fill microvoids in the matrix and also inhibit crack propagation which eventually enhances structural performance [27]. The current investigation studies the synthesis of ZnS nanoparticles by sol–gel auto-combustion approach. Various characterization techniques were used to study the physical properties of the synthesized nanoparticles, evaluate the effect of ZnS incorporation on mechanical properties and thermal degradation behavior of epoxy-based nanocomposites.

MATERIALS AND METHODS

Materials Used

Zinc nitrate hexahydrate ($Zn(NO_3)_2 \cdot 6H_2O$) was purchased from Sigma-Aldrich. Ammonia hydroxide (NH_4OH) was supplied by BDH Chemicals, Thiourea (CH_4N_2S) by Sigma-Aldrich as the sulfur source, and citric acid ($C_6H_8O_7$) was supplied by THOMAS Baker. Epoxy resin type (Nitofill, EPLV) was supplied by Fosroc Company / Jordan, with a density of about 1.04, and used together with its hardener at a mixing ratio of 1:4. The epoxy resin was blended with the hardener in a suitable container to obtain a homogeneous mixture for composite preparation. The volume fractions of the matrix and reinforcement were determined using Eqs. 1 and 2 [28].

$$V_p = \frac{p_c}{p_p} W_p \times 100\% \quad (1)$$

$$V_m = \frac{p_c}{p_m} W_m \times 100\% \quad (2)$$

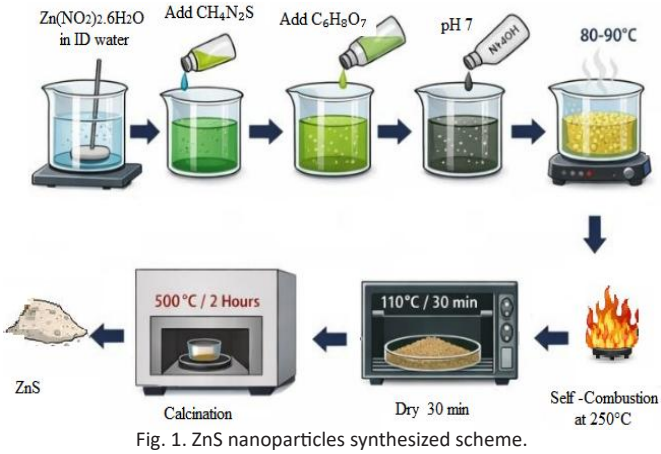

Fig. 1. ZnS nanoparticles synthesized scheme.

Where:

p_c = density of the composite, p_p = density of the particles, ρ_m = density of the matrix, W_m and W_{Pare} the weight fractions of the matrix and the reinforcement, respectively.

Preparation of ZnS

Preparation of ZnS nanoparticles were prepared via the sol–gel auto-combustion technique, as illustrated in Fig. 1. Zinc nitrate hexahydrate ($Zn(NO_3)_2{\cdot}6H_2O$) served as the zinc precursor, thiourea (CH_4N_2S) as the sulfur source, and citric acid ($C_6H_8O_7$) acted as both a chelating agent and fuel. Zinc nitrate was first dissolved in distilled water under continuous magnetic stirring until a clear solution was obtained. Citric acid was then added gradually to form a metal–citrate complex, followed by the addition of thiourea as the sulfur source. The pH of the solution was adjusted to 7 by adding ammonium hydroxide (NH_4OH) dropwise. The resulting solution was heated on a magnetic stirrer at 80–90 °C until a viscous gel was formed. The temperature was then increased to 260 °C, which led to a self -combustion reaction, producing a porous precursor powder. After the combustion process, the obtained powder was dried in an oven at 110 °C for 30 minutes to remove residual moisture from the precursor. Finally, the dried powder was ground thoroughly and calcined at 500 °C for 2 hours in a muffle furnace to improve the crystallinity and obtain pure ZnS nanoparticles.

Preparation of Epoxy /ZnS Nanocomposite

Epoxy nanocomposites reinforced with ZnS nanoparticles were fabricated by hand lay-up at room temperature, as shown in Fig. 2, maintaining an epoxy-to-hardener ratio of 4:1. A (10 × 10) cm mold with a glass base and plastic edges was used. ZnS was incorporated at 0, 1.5, 3, 4.5, and 6 wt%. The resin–ZnS mixtures were sonicated for 25 min in an ultrasonic bath and magnetically stirred for 30 min at room temperature to ensure homogeneous dispersion, after which the hardener was added. Once mixed, the compounds were poured into their molds and degassed to remove trapped air bubbles, before being stabilized chemically under ambient conditions for 15 days complete curing. The post-curing was performed at 60°C for 30 min to make sure that the curing process is complete, the internal stresses are reduced and the moisture absorption is decreased. Specimens were then machined to standard dimensions using a Rapmill 70 CNC machine before they were tested.

Characterization Techniques

In ZnS nanoparticles, the crystal structure was determined by X-ray diffraction (XRD) instrument with Cu Kα radiation (λ = 1.54048 Å)· In addition, Field Emission Scanning Electron Microscopy (FE-SEM) (MIRA3-XMU, TESCAN, Czech Republic) was employed to analyze the surface morphology of the prepared samples.

Thermal Conductivity Test

The Lee disk technique is frequently used to evaluate the thermal conductivity of polymers (see Eqs. 3 and 4) [29]. The sample is positioned between metal disks and an electric heater, and temperature variations are noted until a state of equilibrium is achieved. To quantify thermal

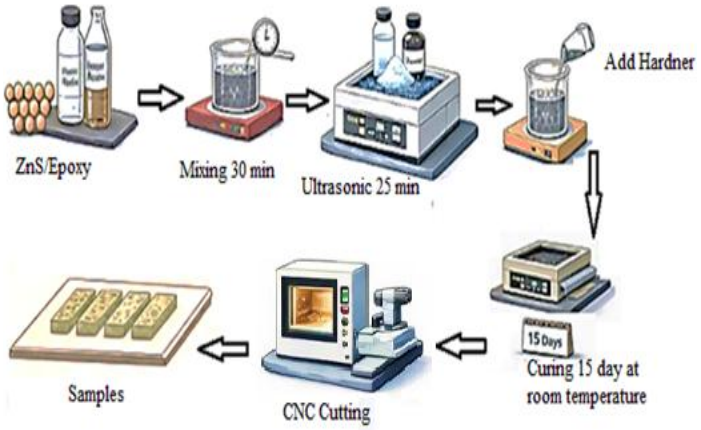

Fig. 2. Epoxy/ZnS nanocomposite fabrication scheme.

conductivity, evaluate material performance, and direct optimization for industrial applications, the results are examined using mathematical formulas including important thermal factors, such as thickness, radius, and temperature. The same Lee disk equations (Eq. 3) are used to measure poorly conductive materials.

$$k\left(\frac{TB-TA}{ds}\right) = e\left[TA + \frac{r}{2}\left(dA + \frac{ds}{4}\right)TA + \frac{1}{2r}ds\ TB\right] \quad (3)$$

e: the amount of thermal energy passing through the unit area of disc material per second (W/m^2. K), calculated from the Eq. 4.

TA¸TB¸TC: disk temperature (A¸B¸C) consequently, quantified in degrees (°C).

d: The disc's thickness in meters (m).

r: The disc's radius in (m).

I: Heater coil current in amps

V: Potential difference, expressed in volts, at both ends of the heating coil.

Hardness Shore D Test

The resistance of a substance's surface to deformation under pressure applied is a typical definition of hardness, which is frequently measured as the ratio of applied force to contact area. Shore hardness was selected for this study because it is appropriate for relatively hard polymeric materials such as epoxy reinforced with nanomaterials. The testing apparatus employed a pointed indenter with a 1.4 mm diameter shank tapering to a 0.1 mm tip and a tip angle of 30°. The indenter applies a controlled pressure to the sample surface and provides a direct digital readout; any deviation from the baseline reading corresponds to the extent of surface damage or scratching on the specimens [30].

Impact Test

In order to conduct the impact resistance test using the «Charpy Test», the sample is placed horizontally and hit with a hammer with a specific weight, and the impact resistance value is calculated using Eq. 5 after the samples are cut into dimensions of (55 mm) in length, and (10 mm) in width, according to the standard specifications for the impact test [31].

$$I \cdot S = \frac{U}{A} \quad (5)$$

Anywhere: I·S: Impact strength (KJ/m^2), A : Cross-sectional area, and U : absorbed energy (KJ).

RESULTS AND DISCUSSION

XRD Analysis of ZnS Nanoparticles

In order to investigate the structural properties of the prepared ZnS nanoparticles, X-ray diffraction (XRD) analysis was carried out. The obtained diffraction pattern is shown in Fig. 3, which exhibits several sharp diffraction peaks indicating the good crystallinity of the synthesized material. The diffraction peaks were observed at 2θ = 28.88°, 47.82°, and 56.66°, corresponding to the crystallographic planes (111), (220), and (311), respectively. Among these peaks, the (111) plane shows the highest intensity, suggesting that the majority of the crystallites are preferentially oriented along this direction. For the planes (111), (220), and (311) corresponding interplanar spacing was observed to be d ≈ 3.089 Å, 1.900 Å, and 1.623 Å respectively. The presence of these diffraction peaks indicates that the synthesized ZnS nanoparticles have a cubic crystal structure with zinc-blende phase, such as in agreement with standard data (JCPDS card No. 05-0566) and literature previously reported [32]. No additional peaks recognize high purity of the material, while peak broadening corresponds to its nanocrystalline nature. The crystallite size (D) was calculated from the Scherrer Eq. 6 [33]:

$$D = 0.9\lambda/(\beta COS\theta) \quad (6)$$

D is the crystallite size, β is the full width at half maximum (FWHM) and θ is the Bragg diffraction angle. The structural parameters derived from the XRD analysis are summarized in Table 1. The crystallite size was 28.549nm, confirming the nanocrystalline nature of ZnS nanoparticles. The calculated lattice parameter values were 5.349 Å, 5.374 Å, and 5.383 Å, which are close to the standard lattice parameter of cubic ZnS (a ≈ 5.41

$$IV = \pi r^2 e(TA + TB) + 2\pi re\left[dATA + \frac{ds}{2}\ (TA + TB) + dBTB + dCTC\right] \quad (4)$$

Å) [34,35].

Morphological Analysis of ZnS Nanoparticles

Fig. 4 shows the FESEM image of the nanosized ZnS sample. The particles appear clustered and agglomerated rather than spherical or regularly faceted, with an average particle size of about 66.87nm. This result is lower than that obtained by Caifeng Wang et al. [36]. The nanosized have a non-uniform surface morphology with a large amount of aggregation and little porosity, as well as an uneven and inhomogeneous size distribution. Additionally, the manufactured samples include some holes, which might be caused by the high exothermic reaction that took place during the combustion event, producing a significant amount of gas in the structure. A similar result was obtained by Alaa Abd Al-Zahra et al. [37]. Subsequently, individual particles may consist of several crystallites with different locations; the

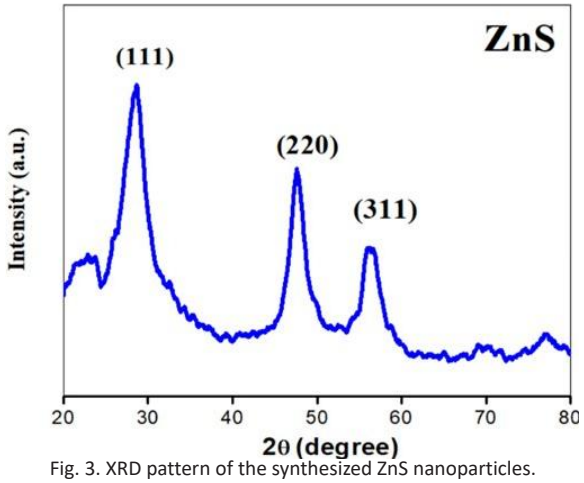

Fig. 3. XRD pattern of the synthesized ZnS nanoparticles.

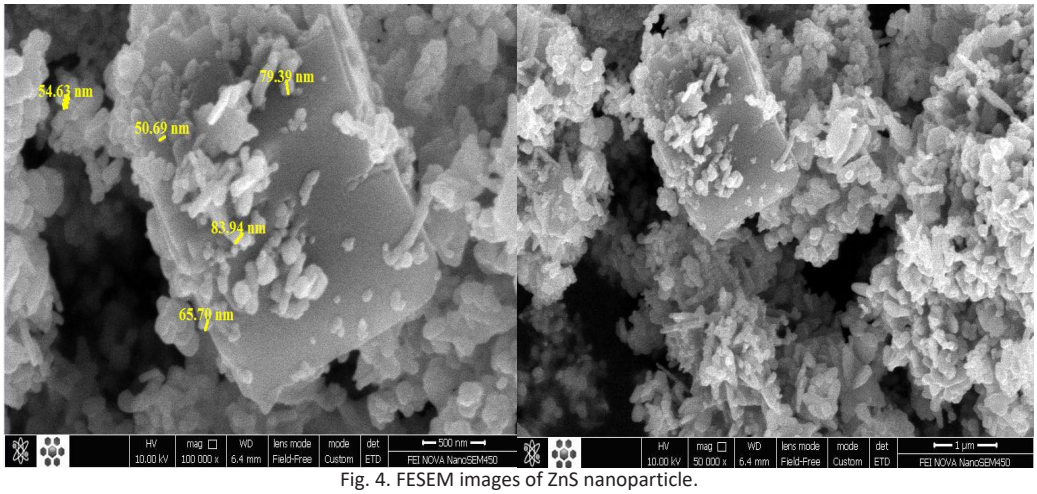

Fig. 4. FESEM images of ZnS nanoparticle.

Table 1. Structural parameters obtained from XRD analysis of ZnS nanoparticle.

2θ (degree)	(hkl)	d-spacing (Å)	FWHM	a (Å)	strain (ε)	δ (nm^{-2})
28.88	(111)	3.08853	0.300	5.349	0.0013	1.23×10^{-4}
47.82	(220)	1.90021	0.240	5.374	0.00095	6.99×10^{-4}
56.66	(311)	1.62308	0.494	5.383	0.0018	2.75×10^{-3}

particle size obtained from FESEM analysis is larger than that estimated from XRD using the Scherrer equation. This variation is related to the polycrystalline nature of the ZnS nanoparticles.

Influence of Different ZnS Nano Additives on Thermal Conductivity

The results of thermal conductivity «K», which was calculated by applying Eqs. 3 and 4, Table 2 shows t that the value of thermal conductivity of epoxy at different reinforcement ratios (0%, 1.5 %, 3%, 4.5 %, and 6%) wt. The Fig. 5 shows that ZnS nanoparticles were efficient in improving the thermal conductivity, as K increases meaningfully with increasing ZnS additive ratio. ZnS has a much higher intrinsic thermal conductivity than

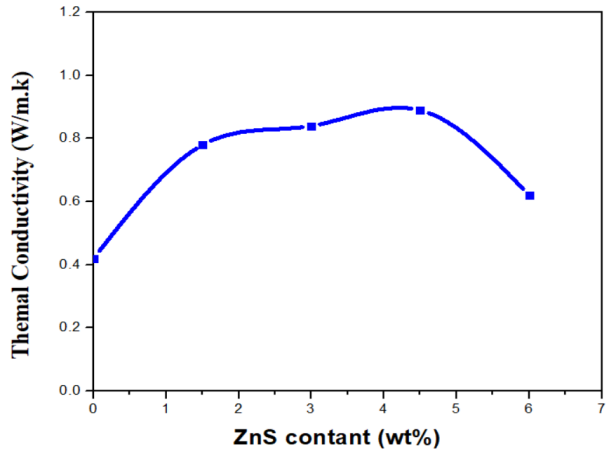

Fig. 5. Thermal conductivity of epoxy nanocomposites as a function of ZnS content (wt%).

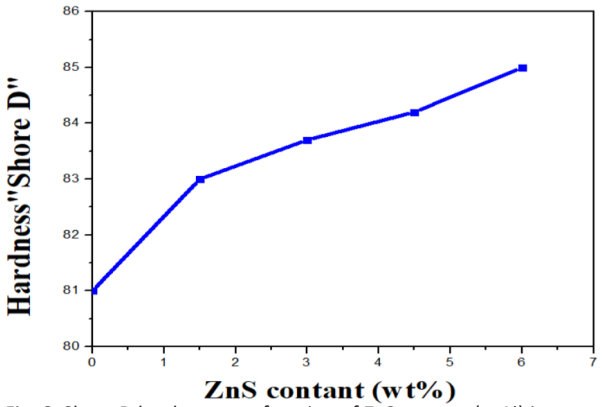

Fig. 6. Shore D hardness as a function of ZnS content (wt%) in epoxy nanocomposites.

Table 2. Thermal conductivity of ZnS /Epoxy nanocomposite.

Samples	Thermal Conductivity Coefficient k(W/m.K)
Pure epoxy	0.42
1.5%ZnS/Epoxy	0.78
3%ZnS/Epoxy	0.84
4.5%ZnS/Epoxy	0.89
6%ZnS/Epoxy	0.62

the epoxy matrix. Introducing ZnS nanoparticles creates additional heat-conducting paths in the composite. Heat can transfer through the continuous epoxy and also across or through ZnS particles, thereby increasing the effective composite thermal conductivity. At low to moderate filler loadings (in which 1.5 to 4.5 wt% was used in this study), nanoparticles get closer and may form at least partial networks or chains [77]. These particle–particle contacts or short paths give rise to heat transport much larger than that of isolated single particles [38], resulting in a drastic rise from 0.42 to ~0.89 W/m·K, while the largest growth (near 4.5%) indicates you reach an effective percolation transition point or an optimal dispersion where many heat-transfer bridges are formed [39].

Shore Hardness Affected of ZnS /Epoxy Nanocomposite

Epoxy samples, with and without ZnS nanocomposite fillers at various weight fractions (0, 1.5, 3, 4.5 and 6 wt%) were tested for Shore D hardness. The aim was to assess the effect of the reinforcement content on hardness for both unfilled and nanoparticle-reinforced epoxy, as presented in Fig. 6. The common conclusion is the incorporation of ZnS nanoparticles into neat epoxy resulted a significant increase in hardness while there was a further improvement when increasing the weight of reinforcement contributed. This improvement is due to the fundamental nature of the nanoparticles such as their morphology, size and intrinsic hardness which allow them to intercalate in through the interstitial regions in polymer chains. The enhanced packing density of the chains, and constrained mobility lead to an overall improvement in hardness of this composite material [40].

Impact Test Affected of ZnS /Epoxy Nanocomposite

The static and rapid loading effects of the epoxy-based nanocomposite materials were assessed as shown in Fig. 7. The reflection is given for the impact strength of various ratios of ZnS nanoparticle addition. The results reveal that the material behaves ductilely under static loading but brittlely during dynamic or fast loading. Using the Charpy impact test, we characterized the fracture energy absorption of neat epoxy resin filled with

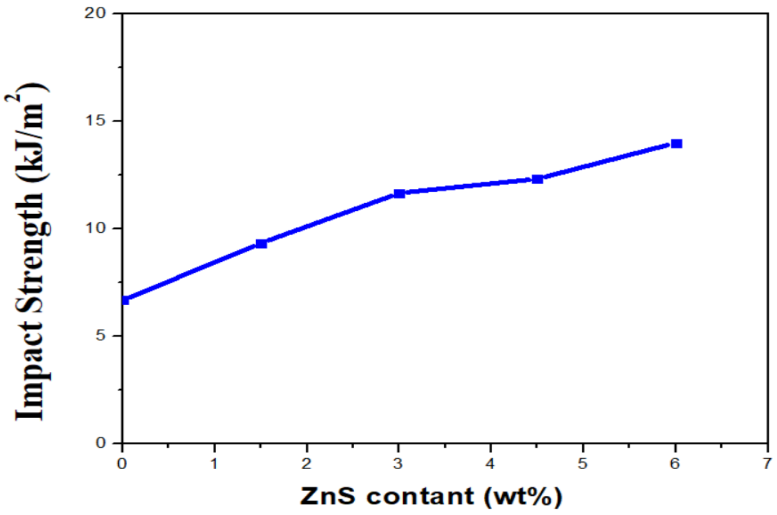

Fig. 7. Impact strength as a function of ZnS content (wt%) in epoxy nanocomposites.

Table 3. Impact value parameters of epoxy /ZnS nanocomposite.

Samples	Thickness (mm)	Width (mm)	Area× 10^{-6} $(m)^2$	Impact Energy (Joule)	Impact Strength (kJ/m^2)
Pure epoxy	0.003	0.01	30	0.2	6.67
1.5%ZnS/Epoxy	0.003	0.01	30	0.28	9.33
3%ZnS/Epoxy	0.003	0.01	30	0.35	11.66
4.5%ZnS/Epoxy	0.003	0.01	30	0.37	12.33
6%ZnS/Epoxy	0.003	0.01	30	0.42	14

ZnS at different nanoparticle weight fractions (0%, 1.5%, 3%, 4.5% and 6%). Table 3 shows the shock resistance values of epoxy and ZnS nanocomposite. For epoxy, failure is attributed to the rupture of inter chain bonds caused by the rapid propagation of initial cracks toward the surface. These inter chain interactions are primarily van der Waals forces, which require relatively low energy to overcome, thereby facilitating crack growth and premature fracture under dynamic loading. Increasing the weight fraction of ZnS nanoparticles improved the mechanical performance of the epoxy by diminishing voids and defects introduced during processing. The nanoparticles serve as effective stress-concentrating sites that impede crack propagation, thereby enhancing the composite's strength [41].

CONCLUSION

ZnS nanoparticles were successfully synthesized via a sol–gel auto-combustion, the process calcination at 500 °C produced a high-purity cubic) ZnS phase .X-ray diffraction (XRD) analysis confirmed the formation of a crystalline cubic ZnS phase with good structural purity and without detectable secondary phases, indicating the successful synthesis of the desired nanomaterial. FE-SEM showed roughly semi-spherical to spherical particles with notable agglomeration. when adequately dispersed in an epoxy matrix can markedly enhance thermal and mechanical performance at relatively low filler loadings. Optimization of particle dispersion and avoidance of agglomeration (particularly at higher loadings) will be important for maximizing property improvements in practical composite applications. Higher hardness and impact resistance make the composite useful for structural adhesives, protective coatings, and over molds where mechanical durability and some thermal conductivity are advantageous.

CONFLICT OF INTEREST

The authors declare that there is no conflict of interests regarding the publication of this manuscript.

REFERENCES

1. Gong H, Chen Z, Yu H, Wu W, Wang W, Pang H, et al. Methane recovery in a combined amine absorption and gas steam boiler as a self-provided system for biogas upgrading. Energy. 2018;157:744-751.
2. D'Amico P, Calzolari A, Ruini A, Catellani A. New energy with ZnS: novel applications for a standard transparent compound. Scientific Reports. 2017;7(1).
3. Saavedra Rodríguez G, Carrillo Torres RC, Sánchez Zeferino R, Álvarez Ramos ME. Stabilized blue emitting ZnS@SiO2 quantum dots. Optical Materials. 2019;89:396-401.
4. Trung DQ, Tran M-T, Hung ND, Nguyen Van Q, Huyen NT, Tu N, et al. Emission-tunable Mn-doped ZnS/ZnO heterostructure nanobelts for UV-pump WLEDs. Optical Materials. 2021;121:111587.
5. R Thistlethwaite L, not provided V. Reproducibility for Thistlethwaite et al. 2020 v1. Springer Science and Business Media LLC; 2020. http://dx.doi.org/10.17504/protocols.io.bka8kshw
6. Karthikeyan B, Arun A, Harini L, Sundar K, Kathiresan T. Role of ZnS Nanoparticles on Endoplasmic Reticulum Stress-mediated Apoptosis in Retinal Pigment Epithelial Cells. Biological Trace Element Research. 2015;170(2):390-400.
7. Kumar P, Maikap S, Singh K, Chatterjee S, Chen Y-Y, Cheng H-M, et al. Highly Reliable Label-Free Detection of Urea/Glucose and Sensing Mechanism Using SiO_2 and CdSe-ZnS Nanoparticles in Electrolyte-Insulator-Semiconductor Structure. Journal of The Electrochemical Society. 2016;163(13):B580-B587.
8. Fu L, Fu Z. Plectranthus amboinicus leaf extract–assisted biosynthesis of ZnO nanoparticles and their photocatalytic activity. Ceramics International. 2015;41(2):2492-2496.
9. Dash CS, Sahoo S, Prabaharan SRS. Resistive switching and impedance characteristics of $M/TiO_{2-x}/TiO_2/M$ nano-ionic memristor. Solid State Ionics. 2018;324:218-225.
10. Dash CS, Prabaharan SRS. Nano Resistive Memory (Re-RAM) Devices and their Applications. REVIEWS ON ADVANCED MATERIALS SCIENCE. 2019;58(1):248-270.
11. Rashki S, Safardoust-Hojaghan H, Mirzaei H, Abdulsahib WK, Mahdi MA, Salavati-Niasari M, et al. Delivery LL37 by chitosan nanoparticles for enhanced antibacterial and antibiofilm efficacy. Carbohydrate Polymers. 2022;291:119634.
12. Mott D, Galkowski J, Wang L, Luo J, Zhong C-J. Synthesis of Size-Controlled and Shaped Copper Nanoparticles. Langmuir. 2007;23(10):5740-5745.
13. Madras G, McCoy BJ. Temperature effects during Ostwald ripening. The Journal of Chemical Physics. 2003;119(3):1683-1693.
14. Slutsker AI, Polikarpov YI, Karov DD, Gofman IV. Energy of the elastic loading of anharmonic solids. Physics of the Solid State. 2013;55(3):668-674.
15. Zeng X, Pramana SS, Batabyal SK, Mhaisalkar SG, Chen X, Jinesh KB. Low temperature synthesis of wurtzite zinc sulfide (ZnS) thin films by chemical spray pyrolysis. Physical Chemistry Chemical Physics. 2013;15(18):6763.
16. Review of Xu et al. Atmos. Chem. Phys. Discuss. (2017). Copernicus GmbH; 2017. http://dx.doi.org/10.5194/acp-2017-483-rc2
17. Zhang Y, Mi L. In Situ Fabrication of Superhydrophobic Zinc Sulfide Films on a Flexible Zinc Foil Substrate. Chemistry Letters. 2012;41(9):915-916.
18. Turgut G, Fahri Keskenler E, Aydın S, Doğan S, Duman S, Sönmez E, et al. A study on characterization of Al/ZnS/p-Si/Al heterojunction diode synthesized by sol–gel technique. Materials Letters. 2013;102-103:106-108.
19. Fischereder A, Martinez-Ricci ML, Wolosiuk A, Haas W, Hofer F, Trimmel G, et al. Mesoporous ZnS Thin Films Prepared by a Nanocasting Route. Chemistry of Materials. 2012;24(10):1837-1845.

20. Singh J, Zhang XL, Hui KS, Hui KN. Corrigendum to "Structural and optical characterization of high-quality ZnO thin films deposited by reactive RF magnetron sputtering" [Mater. Res. Bull. 48 (2013) 1093–1098]. Materials Research Bulletin. 2013;48(5):2010.
21. Yoon Y-G, Choi I-H. Preparation of ZnS thin films by using photoassisted MOCVD. Journal of the Korean Physical Society. 2013;63(8):1609-1614.
22. Figure 22: Accuracy comparison of the proposed FedARCH approach with existing related work (Khan et al., 2022b; Mathivanan et al., 2024; Rasool et al., 2022; Senan et al., 2022; Khan et al., 2022a; Lamrani et al., 2022; Gaur et al., 2022; Vidyarthi et al., 2022; Albalawi et al., 2024; Islam et al., 2023; Viet et al. 2023; Ay, Ekinci and Garip, 2024; Zhou, Wang and Zhou, 2024). PeerJ. http://dx.doi.org/10.7717/peerj-cs.3165/fig-22
23. Kaur N. Thermal Interface materials for efficient heat management in electronics. Applied Thermal Engineering. 2026;287:129415.
24. A. Rajab M. Mechanical properties (Tensile, Hardness and Shock resistance) for the phenol formaldehyde resin with Epoxy resin. DJES. 2019;12(2):35-43.
25. Lu Z, Wu W, Drummer D, Rösel U, Tomiak F, Wang Y, et al. The Micro-Nano Hybrid Filler Al_2O@ CuNPs Is Used to Improve the Thermal Conductivity of Epoxy Resin Composites. Journal of Polymer Science. 2026;64(6):1518-1527.
26. Muthulakshmi M, Sudha AP, Surendhiran S. Synthesis and characterisation of ZnS nanoparticles: a comprehensive study on phase transition and photocatalytic degradation kinetics. Journal of Materials Science: Materials in Electronics. 2025;36(27).
27. Liang M, Wong KL. Study of Mechanical and Thermal Performances of Epoxy Resin Filled with Micro Particles and Nanoparticles. Energy Procedia. 2017;110:156-161.
28. Abdulmajeed AM, Hamzah AF. Experimental Investigation of the Mechanical and Structural Properties of a Functionally Graded Material by Adding Alumina Nanoparticles Using A Centrifugal Technique. Baghdad Science Journal. 2023.
29. Han Z, Fina A. Thermal conductivity of carbon nanotubes and their polymer nanocomposites: A review. Progress in Polymer Science. 2011;36(7):914-944.
30. Alraziqi ZNR. Water Temperature Effect on Hardness and Flexural Strength of (PMMA/TiO_2 NPs) for Dental Applications. Baghdad Science Journal. 2022;19(4):0922.
31. Ahmade NS, Abdullah HW, Abduallah SS, Abdullah RM. Fabrication, characterization and some mechanical properties of graphene–kevlar epoxy hybrid. AIP Conference Proceedings: AIP Publishing; 2020.
32. Omidi A, Habibi-Yangjeh A. Microwave-assisted method for preparation of Sb-doped ZnO nanostructures and their photocatalytic activity. Journal of the Iranian Chemical Society. 2013;11(2):457-465.
33. Abdullah HW, Mubarak TH, Resan KK. Graphene Oxide Nano-Sheets: A Novel Eco-Friendly Approach for Tissue Engineering and Antibacterial Applications in Bone Disease. Science and Technology Indonesia. 2024;9(4):806-817.
34. Mohan R, Jayamoorthy K. Ni-doped ZnS nanoparticles encapsulated in polypropylene glycol: exploring synthesis, structural integrity, optical behavior and thermal stability. Journal of Materials Science: Materials in Electronics. 2025;36(25).
35. Baruah JM, Kalita S, Narayan J. Green chemistry synthesis of biocompatible ZnS quantum dots (QDs): their application as potential thin films and antibacterial agent. International Nano Letters. 2019;9(2):149-159.
36. Wang C, Li Q, Hu B. Preparation and characterization of ZnS nanoparticles prepared by hydrothermal method. International Journal of Modern Physics B. 2017;31(16-19):1744055.
37. Al-Ghamdi AA, Al-Ghamdi AA, Al-Hartomy OA, Nawar AM, El-Gazzar E, El-Tantawy F, et al. Novel photoconductive Ag/nanostructure ruthenium oxide/p-type silicon Schottky barrier diode by sol–gel method. Journal of Sol-Gel Science and Technology. 2013;67(2):368-375.
38. Al Dayyeni A, Al-Gailani B, Mahdi M. The role of erythropoietin levels and other hematological factors in the diagnosis of polycythemia vera in Iraqi patients. Iraqi Journal of Hematology. 2023;12(1):50.
39. Mahmood OA, Jameel ZN, Abdullah HW. Effect of Different Multi-Walled Carbon Nanotubes MWCNTs on Mechanical and Physical Properties of Epoxy Nanocomposites. IOP Conference Series: Materials Science and Engineering. 2021;1094(1):012166.
40. Mohammed IS, Mansoor JM, Abdullah HW, Habeeb AA. Impact of ZnO nanoparticles on mechanical and dielectric properties of epoxy resin composites. AIP Conference Proceedings: AIP Publishing; 2023. p. 090013.
41. Abdullah AN, Abeduljabbar NF. Preparation of Nanoparticles and Study of the Effect of Some of Their Physical Properties on Epoxy Polymer. Al-Bahir. 2025;6(2).